Received: 24 August 2022 | Revised: 8 November 2022 | Accepted: 10 December 2022

DOI: 10.1002/cne.25449

RESEARCH ARTICLE

JCN RESEARCH IN SYSTEMS NEUROSCIENCE THE JOURNAL OF COMPARATIVE NEUROLOGY WILEY

Architecture of the inferior parietal cortex in capuchin monkey

Vânio Bonfim[1,2] | Andrei Mayer[2,3] | Márcio L. Nascimento-Silva[1,2] | Bruss Lima[1] | Juliana G. M. Soares[1] | Ricardo Gattass[1]

[1]Laboratory of Cognitive Physiology, Instituto de Biofísica Carlos Chagas Filho, Universidade Federal do Rio de Janeiro, Rio de Janeiro, Brazil

[2]Laboratory of Neurobiology II, Instituto de Biofísica Carlos Chagas Filho, UFRJ, Rio de Janeiro, Brazil

[3]Mayer Laboratory, Universidade Federal de Santa Catarina, Florianópolis, Santa Catarina, Brazil

Correspondence
Prof. Ricardo Gattass, Laboratory of Cognitive Physiology, Instituto de Biofísica Carlos Chagas Filho, Bloco G, CCS, Rio de Janeiro, RJ 21941-900, Brazil.
Email: rgattass@gmail.com

Funding information
Fundação Carlos Chagas Filho de Amparo à Pesquisa do Estado do Rio de Janeiro, Grant/Award Numbers: E-26/110.905/2013, E-26/210.917/2016; Financiadora de Estudos e Projetos, Grant/Award Number: PEC20150 (0354/16); Conselho Nacional de Desenvolvimento Científico e Tecnológico, Grant/Award Numbers: 471.166/, 2013, -8

Abstract

We studied the organization of the inferior parietal cortex (IPC) in five capuchin monkey (6 hemispheres) using cytoarchitectonic (Nissl), myeloarchitectonic (Gallyas), and immune-architectonic (SMI-32 monoclonal antibody) techniques. We partitioned the IPC into five distinct areas: PFG, PG, Opt, PFop, and PGop. Since we used parasagittal sections, we were not able to study area PF due to its far lateral position, which yielded slices that were tangential to the pial surface. Areas PFG, PG, and Opt were in the convexity close to the lateral sulcus, while PFop and PGop were positioned more posteriorly, in the opercular region of IPC. Of all the five regions, area Opt was the one most similar to its analogue in the macaque, especially as revealed with SMI-32 staining. Namely, in both primate species area Opt showed a low density of large pyramidal neurons. Additionally, the apical dendrites of these neurons were sparse and vertically orientated, resembling columns. We also found area PG to be similar: both species exhibited cell body layers with a radial arrangement. On the other hand, Nissl staining revealed area PFG to be architectonically different between New and Old-World monkeys: PFG in the capuchin showed a comparatively higher cell density than in macaques, especially in layers II and IV. These results suggest that evolution may have enabled the functional specialization of these brain regions based on behavioral demands of upper limb use. The small differences in the IPC of the two primates may be linked to interspecies variability.

KEYWORDS
anatomy of the inferior parietal lobe, capuchin monkey, RRID:AB_509998, somatosensory association cortex

1 | INTRODUCTION

Skilled hand movements and tool manipulation are landmarks abilities observed in capuchin monkeys (Mayer et al., 2016, 2019; Wright et al., 2015). These skills allow individuals to accurately interact with and modify the external environment in accordance with their need. The correct performance of such behaviorally relevant tasks depends on different regions of the parietal cortex that process and integrate sensory inputs from the body and the environment (Kalaska & Rizzolatti, 2013; Niu et al., 2021; Rozzi et al., 2008). These areas process sensory information from different modalities (i.e., somatosensory, visual and auditory information) and are highly connected to motor areas in the frontal lobe. The frontal lobe, in turn, implements the motor planning and execution according to the goal of the task and the available sensory information (Geyer et al., 2005; Passarelli et al., 2021; Rizzolatti et al., 1997).

The monkey's inferior parietal cortex (IPC) is a region of the neocortex limited medially/dorsally by the intraparietal sulcus and laterally/ventrally by the lateral and superior temporal sulci (Fogassi & Luppino, 2005; Rizzolatti et al. 1998). The IPC was first described in the early 20th century by Brodmann (1905). He used the Nissl method to partition the cerebral cortex in several areas (Vogt & Gabriel, 1993;

Zeki, 2005). Brodmann described the IPC as being a single cytoarchitectonic area, named area 7 (Figure 1a). About a decade later, Vogt and Vogt (1919) used cyto- and myeloarchitecture techniques to divide the IPC into caudal and rostral sectors. The caudal two-thirds of IPC was called area 7a, and the rostral one-third of IPC was named area 7b (Figure 1b). Later, von Economo and Koskinas (1925) revised the nomenclature proposed by Vogt and Vogt (1919). They maintained the same parcellation, but used the numerical nomenclature proposed by Brodmann (1905) followed by letters. Von Bonin and Bailey (1947) also maintained the same subdivision as Vogt and Vogt (1919), but renamed area 7b as PF and 7a as PG (Figure 1c). However, subsequent anatomical, connectivity and functional studies use the PF, PFG, PG and Opt parcellation (Andersen et al., 1990a, 1990b, 1997; Asanuna et al., 1985; Buneo & Andersen, 2006; Clower, 2001; Friedman & Goldman-Rakic, 1994; Jones & Burton, 1976; Leinonen et al., 1979a, 1979b; Lewis & Van Essen, 2000; May & Andersen, 1986; Rushworth et al., 1997a, 1997b; Stanton et al., 2005; Yokochi et al., 2003), despite the fact that Preuss and Goldman-Rakic (1991) and Rozzi et al. (2006) preserve the 7a and 7b nomenclature. Toward the end of the 20th century, Pandya and Seltzer (1982) carried out an influential study (Figure 1d) based on neuronal connectivity and architecture, which demonstrated that the IPC can be subdivided into six areas: PF and PFG rostrally, PG and Opt dorsally, and two more ventrally located subdivisions PGop (caudal) and PFop (rostral). Subsequently, Preuss and Goldman-Rakic (1991) proposed a different parcellation, with only a single area in the parietal operculum, 7op, and three areas on the IPL convexity, rostral area 7b, followed caudally by areas 7a-m and 7a-l (Figure 1e). More recent studies, employing the methods of Nissl, Gallyas, immunohistochemistry with SMI-32 monoclonal antibody (Figure 1f) and multimodal receptor architectonic techniques (Figure 1g) confirmed the accuracy of Pandya and Seltzer (1982) original parcellation of the IPC (Geyer et al., 2005; Gregoriou et al., 2006; Niu et al., 2021; Rozzi et al., 2006).

It is well known that the inferior parietal cortex (IPC) is involved in the sensorimotor integration underlying hand movements. Assuming that primates with comparable manual skills share similar cortical circuits, we tested the hypothesis that the architectural organization of the IPC in the New-World capuchin monkey is similar to the one previously described for the Old-World macaque monkey. To this aim, we used neuronal and fiber staining techniques (the Nissl and Gallyas methods, respectively) and immunohistochemistry labeling with the monoclonal SMI-32 antibody to characterize the architectural features of the cortical areas that compose the capuchin monkey IPC.

2 | METHODS

2.1 | Animals

In this study, we used 6 hemispheres (3 right and 3 left hemispheres) of 5 capuchin monkeys (*Sapajus* s.p., formerly called *Cebus* s.p.). All subjects were adults (3 males and 2 females) weighing between 2.4 and 4.4 kg. All experimental procedures were approved by the Ethics Committee for the Care and Use of Experimental Animals (CEUA-CCS protocol # IBCCF-119, Center for Health Science, Federal University of Rio de Janeiro), and were also in accordance with the guidelines of the National Institute of Health for the Care and Use of Laboratory Animals (NIH-USA).

2.2 | Perfusion and microtomy

A lethal dose of sodium pentobarbital was administered to the animals intravenously. After reaching deep anesthesia, the animals were submitted to perfusion through the heart with 0.9% saline, followed by 4% paraformaldehyde in phosphate buffer (pH 7.3), 4% formaldehyde in 2.5% sucrose phosphate buffer, 4% paraformaldehyde in 5% sucrose phosphate buffer and, finally, in 10% sucrose phosphate (pH 7.2–7.4). After perfusion, the brain was removed from the skull and placed in a postfixation solution of 4% paraformaldehyde in 30% sucrose for approximately 24 h. After this postfixation period, the brain was sectioned (40 or 50 μm thick slices) in the parasagittal plane at using a cryomicrotome (Cryostat, Bright Instruments Inc.).

2.3 | Histological processing

Alternate histological sections were stained for cell bodies (Nissl method), myelinated fibers (Gallyas method as described in Gallyas, 1979), or neurofilaments M and H of pyramidal neurons (immunohistochemistry with SMI-32 monoclonal antibody) (Campbell & Morrison, 1989; Hof et al., 1996; Sternberger & Sternberg, 1983).

For SMI-32 immunohistochemistry, individual free-floating sections were placed in separate wells and washed three times with 0.1 M saline phosphate buffer (PBS) for 10 min. Subsequently, the slices were incubated with 2% bovine serum albumin (BSA) in a solution of 0.3% triton X-100 in PBS (PBS-Tx), for 1 h at room temperature. After three washes in PBS, sections were kept under gentle agitation overnight at room temperature in a solution containing the mouse monoclonal SMI-32 antibody (1:5000 dilution, Covance Research Products Inc. Cat# SMI 32R-500, RRID: AB_509998) in 2% BSA and 0.3% PBS-Tx. The sections were washed three times in PBS, incubated with biotinylated anti-mouse secondary antibody (1:200 dilution, Vector Laboratories) for 2 h at room temperature. Subsequently, they were washed with PBS (3 times for 10 min) and incubated for 1 h in Vectastain Elite brand avidin-biotin complex (avidin biotincomplex-ABC) (1:500 dilution, Vector Laboratories) at room temperature. Immunoreactivity was revealed with a 0.05% solution of 3,3'-diaminobenzidine (DAB) and 0.1% nickel ammonium sulfate. The sections were then mounted on bi-gelatinized slides (1% gelatin), dehydrated in increasing amounts of alcohol (75%, 90%, 100%, and again 100%) for 1 min in each of the solutions, clarified with xylene (twice for 3 min), covered with DPX (BDH Laboratory Supplies, Poole, BH15 1TD, England), and then mounted with a glass coverslip.

2.4 | Architectural analysis

We first selected, based on anatomical landmarks such as the central, intraparietal and lateral sulci, the histological sections that contained

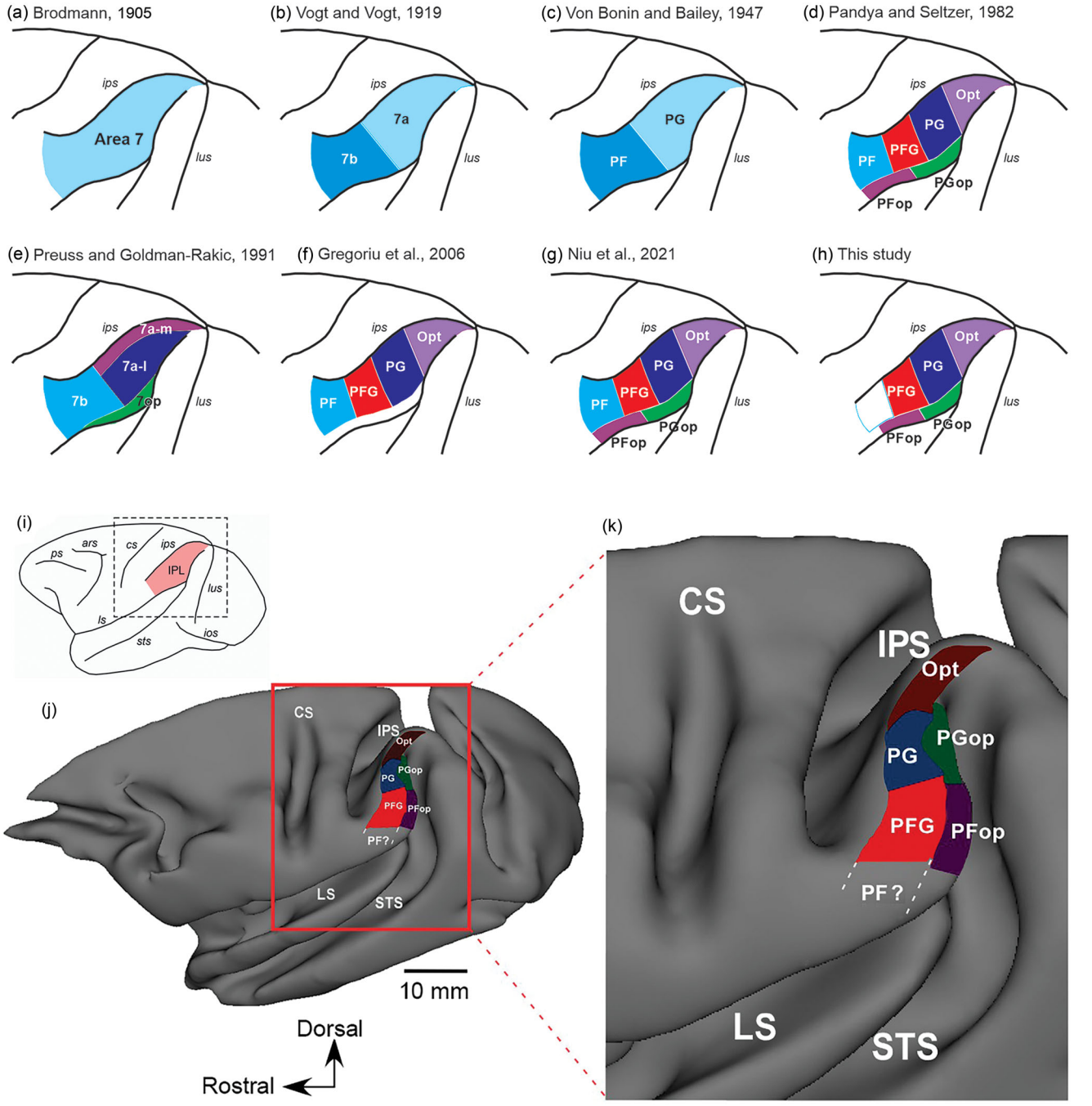

FIGURE 1 Architectonic subdivisions of the inferior parietal cortex (IPC). (a–e) Subdivisions of the macaque monkey IPC as described by (a) Brodmann (1905), (b) Vogt & Vogt (1919), (c) Von Bonin & Bailey (1947), (d) Pandya & Seltzer (1982), (e) Preuss & Goldman-Rakic (1991), (f) Gregoriu et al., 2006, (g) Niu et al., 2021. (h) Subdivision proposed by the present study for the capuchin monkey IPC. (i) Lateral view of the monkey brain showing the portion of the left cortex (dashed square) that is enlarged in panels a–h. (j) Architectural subdivision of the capuchin monkey IPC in a 3D reconstruction of the left hemisphere of the Case 1. Five architectural areas are illustrated: three areas in the IPC convexity (PFG, in red; PG, in blue; and Opt, in brown), and two areas in the IPC operculum (PFop, in purple; and PGop, in green). The reconstruction was done with the aid of the CARET software and is based on the areal contours estimated at the level of layer 4, thus accentuating the opening of the sulci. (k) Magnification of the region of interest delimited by the red rectangle in j. Sulci: arcuate (ars), central (cs), inferior-occipital (ios), intraparietal (ips), lateral (ls), lunate (lus), principal (ps), and superior temporal (sts)

the cortical regions of interest. These sections were microphotographed with the aid of the 2D "virtual tissue" module of the Neurolucida system (MBF Biosciences, Inc, RRID: nif-0000-10294, Williston, VT, USA). We used the graphics program Canvas 15 (ACD Systems International Inc., RRID:SCR_014288/ Fort Lauderdale, FL, USA, Victoria, BC, Canada) to visualize the images on a computer screen at different amplifications (25%, 50%, 100%, and 200%). Based on these images we carried out the architectural analysis of the capuchin IPC.

2.5 | Three-dimensional (3D) reconstruction of anatomical data

The 3D reconstruction of the IPC convexity with its corresponding cortical areas was obtained for the left hemisphere of case R13-01 using the CARET software (Computerized Anatomical Reconstruction and Editing Tool Kit, available at http://brainvis.wustl.edu/wiki/index.php/Caret:Download), which is widely used in neuroanatomical studies (Bezgin et al., 2008; Bezgin et al., 2012; Chaplin et al, 2013; Galletti et al., 2005; Kalwani et al., 2009; Sperka & Ditterich, 2011; Van Essen, 2005; Van Essen, 2012; Van Essen et al., 2001; Zhong et al., 2010). First, we used histological sections immunoreacted for SMI-32 to identify layer IV. The outline of layer IV was digitized using Neurolucida. Subsequently, the anatomical boundaries between different cortical areas were identified and marked. This procedure was carried out for all available sections and the corresponding images were appropriately aligned. The resulting XML file was edited in two steps. In the first step, the XML file was duplicated: one containing the x, y and z coordinates of layer IV outline, and the other containing the *x*, *y*, and *z* coordinates of the markers (features of the Neurolucida) corresponding to the anatomical limits of the cortical areas. In the second step, the file containing the *x*, *y*, and *z* coordinates of the markers were organized and converted by a homemade Python program into a file format that could be read by the CARET program. Finally, within CARET we were able to obtain a 3D reconstruction of the capuchin IPC partitioned in accordance with the steps described above.

3 | RESULTS

This work comprises a qualitative assessment of IPC architecture, through the analysis of histological sections of six hemispheres of five adult capuchin monkeys. The illustrations shown below correspond to microphotographs of histological sections of the left hemispheres of cases R13-01 (Nissl and SMI-32) and CB-78 (Gallyas), which are exemplar for all hemispheres analyzed. The architectural borders of the IPC areas could be identified at low magnification (5× objective) based on the differential staining intensity for cell bodies, myelin fibers and SMI-32 immunohistochemistry. We also analyzed microphotographs at higher magnification (10× objective), where more detailed architectural features, such the staining pattern and staining intensity of cell bodies and their corresponding cell processes (including neuropil), could be observed.

After careful architectural analysis, we verified that the organization of IPC areas was similar to the one previously described in the macaque by Pandya and Seltzer (1982). We thereby adopted the same nomenclature proposed by these authors. Moreover, we identified and characterized five cortical areas in the capuchin monkey IPC. Three of them, PFG, PG, and Opt, are located in the convexity of the IPC, while the other two areas, PFop and PGop, are in the IPC operculum. It is possible that there is a sixth cortical area, PF, which was not analyzed in this study. The reason for this is that we sliced the brain in the parasagittal plane. Since area PF is located laterally in the brain, the histological slices corresponding to area PF were too tangential to be appropriately analyzed.

3.1 | Delimitation of IPC areas in the capuchin monkey

Figure 1h, j, and k shows the location of the five IPC areas identified in this study: PFG, PG, Opt, PFop, and PGop. Area PFG, the most lateral of the analyzed areas, is located in the posterior bank of the intraparietal sulcus and it borders posteriorly with area PFop and medially with area PG. Its lateral limit is parallel to the lateral tip of the intraparietal sulcus. Area PFop is limited rostrally by area PFG and posteriorly by the anterior margin of the superior temporal sulcus, close to the convergence with lateral sulcus. Its lateral boundary lies near to the medial tip of the lateral sulcus. Medially, PFop is bordered by area PGop. Area PGop extends caudally up to the crown of the anterior bank of the superior temporal sulcus.

On the mediolateral axis, area PG lies between area PFG, located laterally, and area Opt, located medially. PG is also located close to the posterior bank of the intraparietal sulcus, and its posterior border is shared with area PGop. Area PGop, which is located close to the anterior bank of the superior temporal sulcus, is bordered laterally by PFop and medially by Opt. Opt is the most medial and dorsal area of the IPC, being located on the convexity immediately posterior to the intraparietal sulcus. The caudal limit of Opt is located close to the dorsal tip of the superior temporal sulcus and the dorsocaudal tip of the intraparietal sulcus. Most of the lateral border of Opt is shared with area PG, and a very small portion is shared with area PGop.

3.1.1 | Areas PFG and PFop

In Nissl-stained sections (Figures 2a and 5), we observed that area PFG has a high cell density. At the limit of layer II, the cells are not arranged in a palisade, as it is usually characteristic of this cortical layer. Layer III stands out as presenting a stratification into superficial (a), intermediate (b) and deep (c) sublayers. The superficial sublayer shows a high density of predominantly small cell bodies. The intermediate sublayer exhibits predominantly medium-sized and sparse cell bodies. The deep sublayer contains predominantly large and sparse cell bodies. On the other hand, layer IV is thick and shows poorly defined limits with layer V. Layer V also presents medium and large cell bodies, but these are

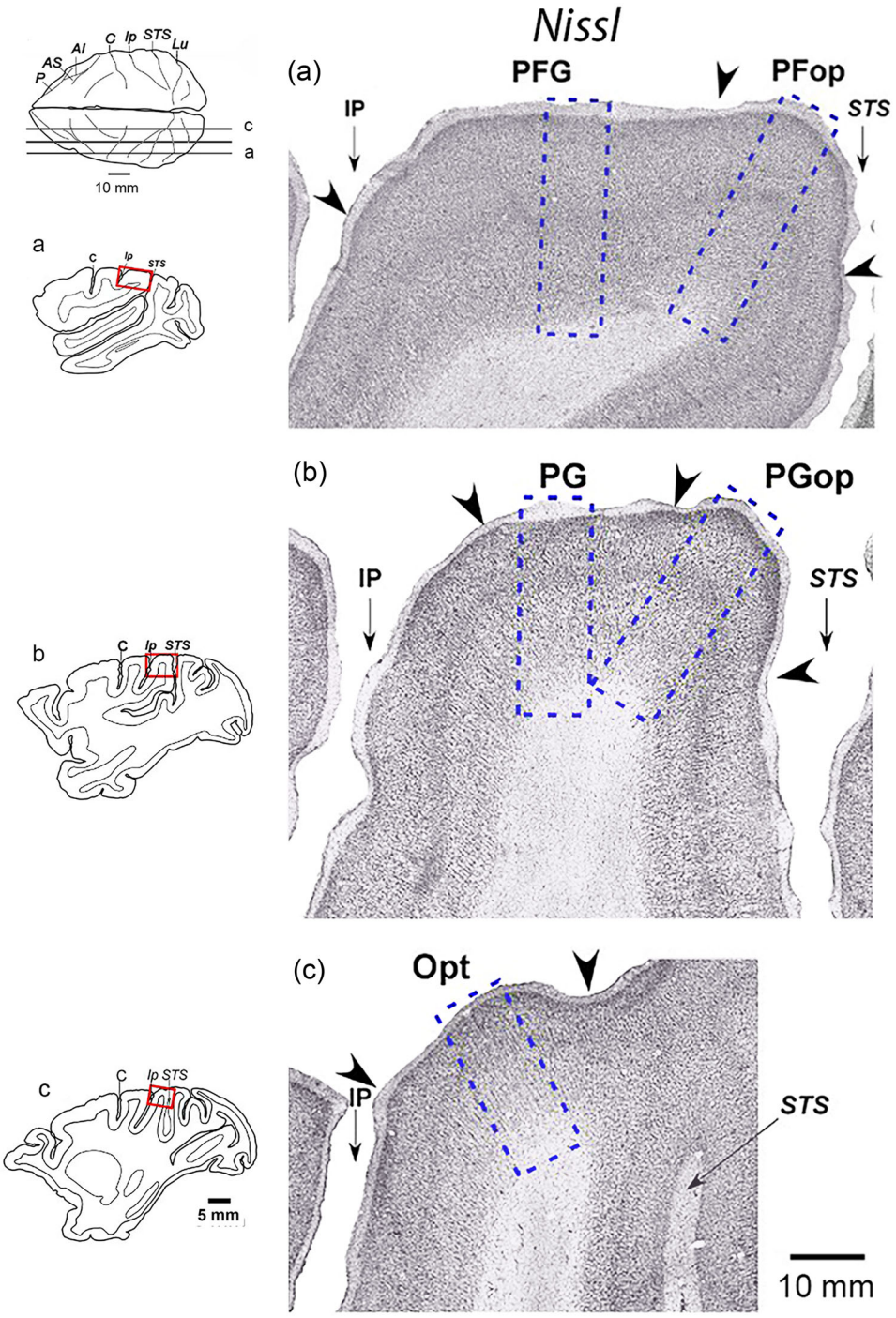

FIGURE 2 Characterization of areas PFG, PG, PGop, PFop, and Opt based on cytoarchitecture. Left: histological sections (a–c) running from lateral to medial, with (a) being the lateralmost section. Arrowheads indicate the borders of areas PFG, PG, PGop, PFop, and Opt. **Right**: schematic drawings of the three parasagittal sections indicated in a–c, with a red rectangle indicating the region that is enlarged in the photomicrographs. The levels of the parasagittal sections used for analysis are indicated by lines in the schematic drawing of the dorsal view of the capuchin brain (top left). Abbreviations as in Figure 1

homogeneously distributed. Finally, layer VI shows a predominance of neurons with small cell bodies.

Immunohistochemistry for SMI-32 (Figures 3a and 5) reveals a clear pattern of lamination in IPC. Labeling is particularly intense in layers III and V, which present large immunoreactive cell bodies. Layers I, II, and IV show very weak immunostaining, even though layers II and IV are often invaded by apical dendrites originating from cells located in layers III and V, respectively. Layer VI usually presents more immunostaining of neuropil than of cell bodies. Area PFG is less immunostained than the immediately neighboring cortical regions. Additionally, we

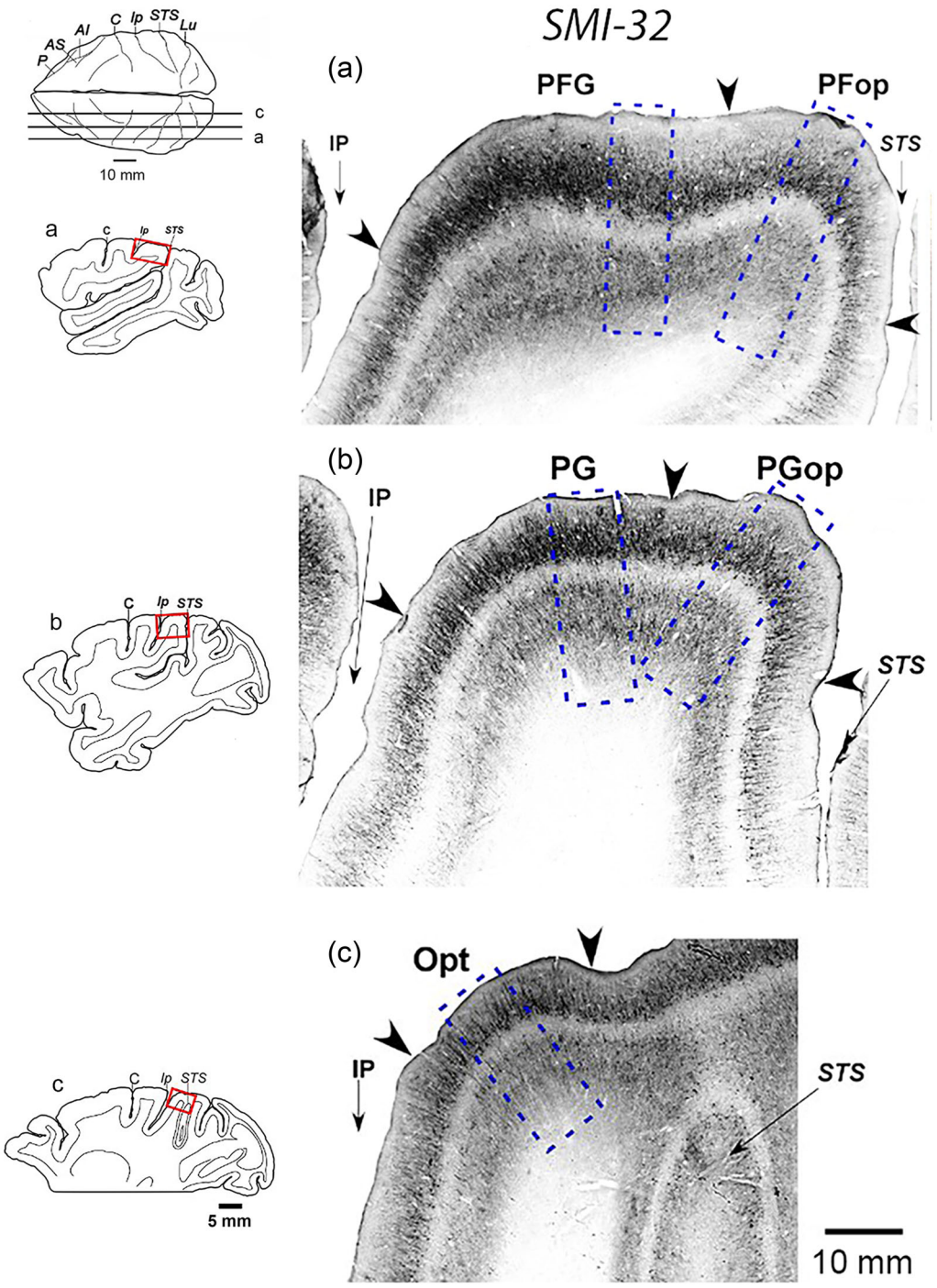

FIGURE 3 Characterization of areas PFG, PG, PGop, PFop, and Opt based on SMI-32 immunostaining. Left: histological sections (a–c) running from lateral to medial, with (a) being the lateralmost section. Arrowheads indicate the borders of areas PFG, PG, PGop, PFop, and Opt. **Right**: schematic drawings of the three parasagittal sections indicated in a–c, with a red rectangle indicating the region that is enlarged in the photomicrographs. The levels of the parasagittal sections used for analysis are indicated by lines in the schematic drawing of the dorsal view of the capuchin brain (top left). Abbreviations as in Figure 1

also observe a clear distinction between its layers V and VI. Layer III is intensely labeled and predominantly populated by sparse cells of medium and large size, especially in the sublayer c, which also exhibits neurons with short apical dendrites. Layer V staining presents a low density of small and medium cells, while layer VI presents small and sparse cells with immunostained neuropil.

In myelin-stained sections, area PFG is characterized by having a layer I with few fibers. Additionally, layers II and III are lightly stained and have visible outer and inner bands of Baillarger. The deep layers are more myelinated than superficial layers (Figures 4a and 5).

In Nissl-stained sections (Figures 2a and 6), layers II and IV of area PFop stand out for being more intensely stained than layers II and IV

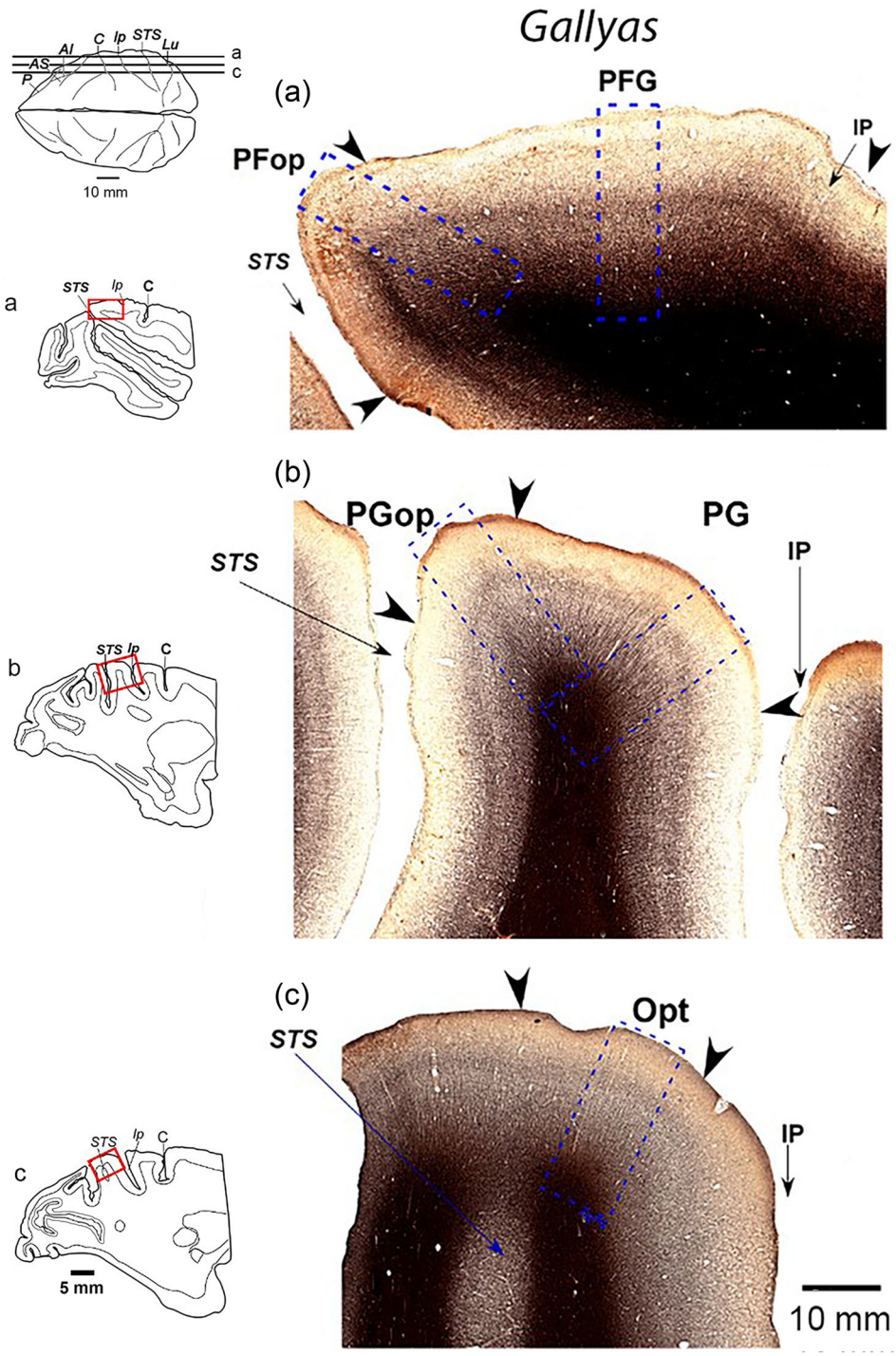

FIGURE 4 Characterization of areas PFG, PG, PGop, PFop, and Opt based on myeloarchitecture. Left: Histological sections (a–c) running from lateral to medial, with (a) being the lateralmost section. Arrowheads indicate the borders of areas PFG, PG, PGop, PFop and Opt. **Right**: schematic drawings of the three parasagittal sections indicated in a–c, with a red rectangle indicating the region that is enlarged in the photomicrographs. The levels of the parasagittal sections used for analysis are indicated by lines in the schematic drawing of the dorsal view of the capuchin brain (top left). Abbreviations as in Figure 1

of PFG. This characteristic enabled us to draw a clear border between areas PFop and PFG. In addition to its stronger staining, layer II of area PFop is thinner than the one of PFG. Moreover, due to the classic palisade arrangement of the granular neurons cell bodies in layer II, especially at its most superior border, we are able to draw a clear distinction between layers I and II of PFop. As we did for PFG, we also stratified Layer III of PFop into three sublayers (a, b, and c). However, sublayer IIIc of PFop is comparatively more lightly stained and shows fewer of the large pyramidal cells that we observed in sublayer IIIc of PFG. Layer IV of PFop is more intensely labeled than layer IV of PFG,

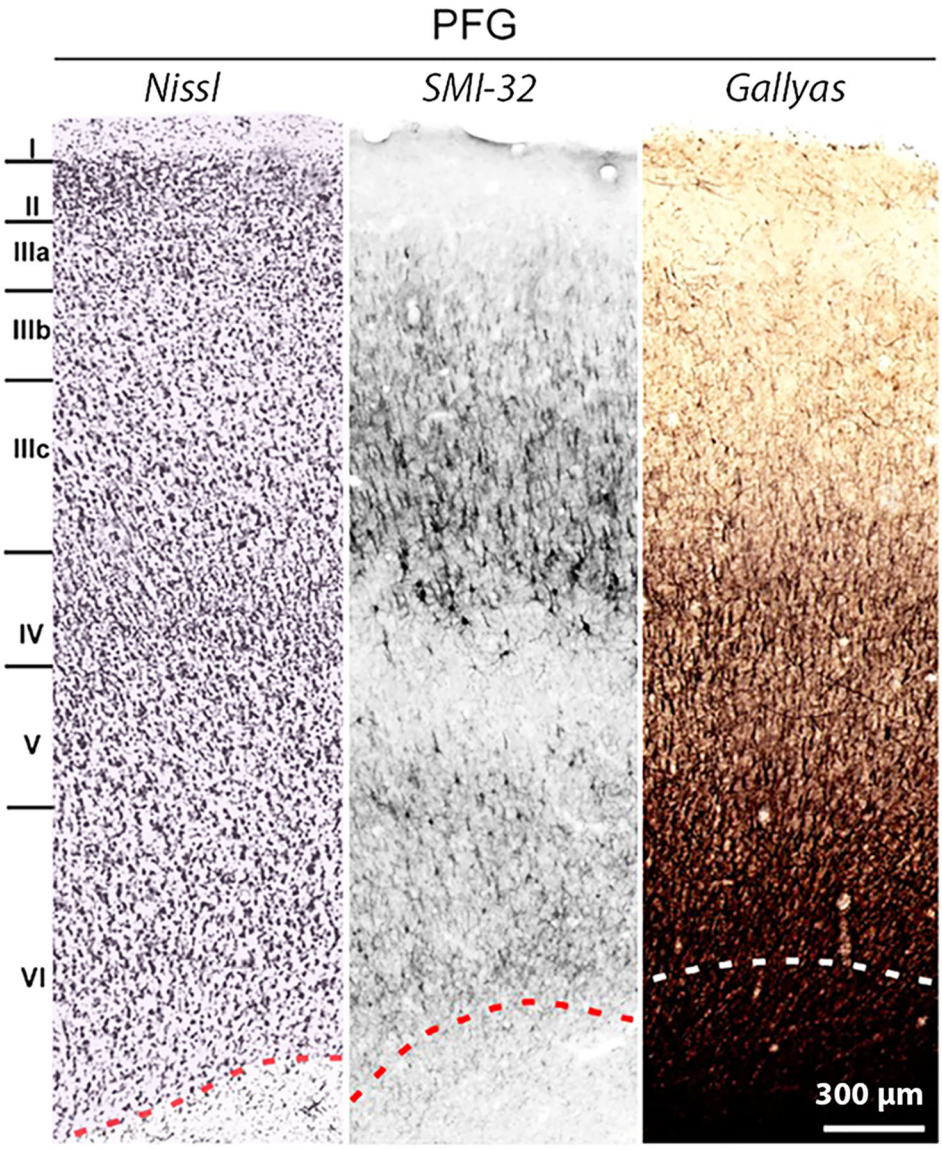

FIGURE 5 Characterization of area PFG based on cytoarchitecture, SMI-32 immunostaining and myeloarchitecture. Enlargement of the regions of area PFG encompassed by the blue dashed rectangles shown in Figures 2–4. Red or white dashed lines indicate the boundary between gray and white matters

while layer V of PFop is less dense in medium and large sized cell bodies than area PFG. This made it more difficult to draw a clear boundary between layers IV and V.

We analyzed the SMI-32 immunostaining pattern for areas PFG and PFop (Figures 3a and 6). Layer III of area PFop contained medium and large cells that were less scattered in sublayer c, as compared to the same sublayer in PFG. However, we observe thin apical dendrites that are comparatively more apparent in PFop. These differences may be related to the fact that layer III is thinner in PFop, although we must keep in mind that differences in layer thickness can also be partially explained by differences in the plane of cut with respect to the orientation of the cortical mantle. We find small and medium pyramidal cells scattered along Layer V of PFop, but with more apparent apical dendrites than observed in layer V of PFG. In PFop, layer VI contained fewer cells and apical dendrites than layer V, even though it showed intense neuropil labeling.

In myelin-stained sections, area PFop is characterized by a radial appearance of fibers. This area presents weak myelin labeling in layers I and II and a light labeling in layer III. Layers IV, V, and VI are all well stained. We are also able to visualize the outer and inner bands of Baillarger. However, their boundaries are less prominent than the ones observed in PFG (Figures 4a and 6).

3.1.2 | Areas PG and PGop

Layer IV, as evidenced by Nissl staining, is clearly visible in area PG, even at low magnification (Figure 2b). Indeed, this layer was more intensely stained in area PG as compared to PFG (compare Figure 2a

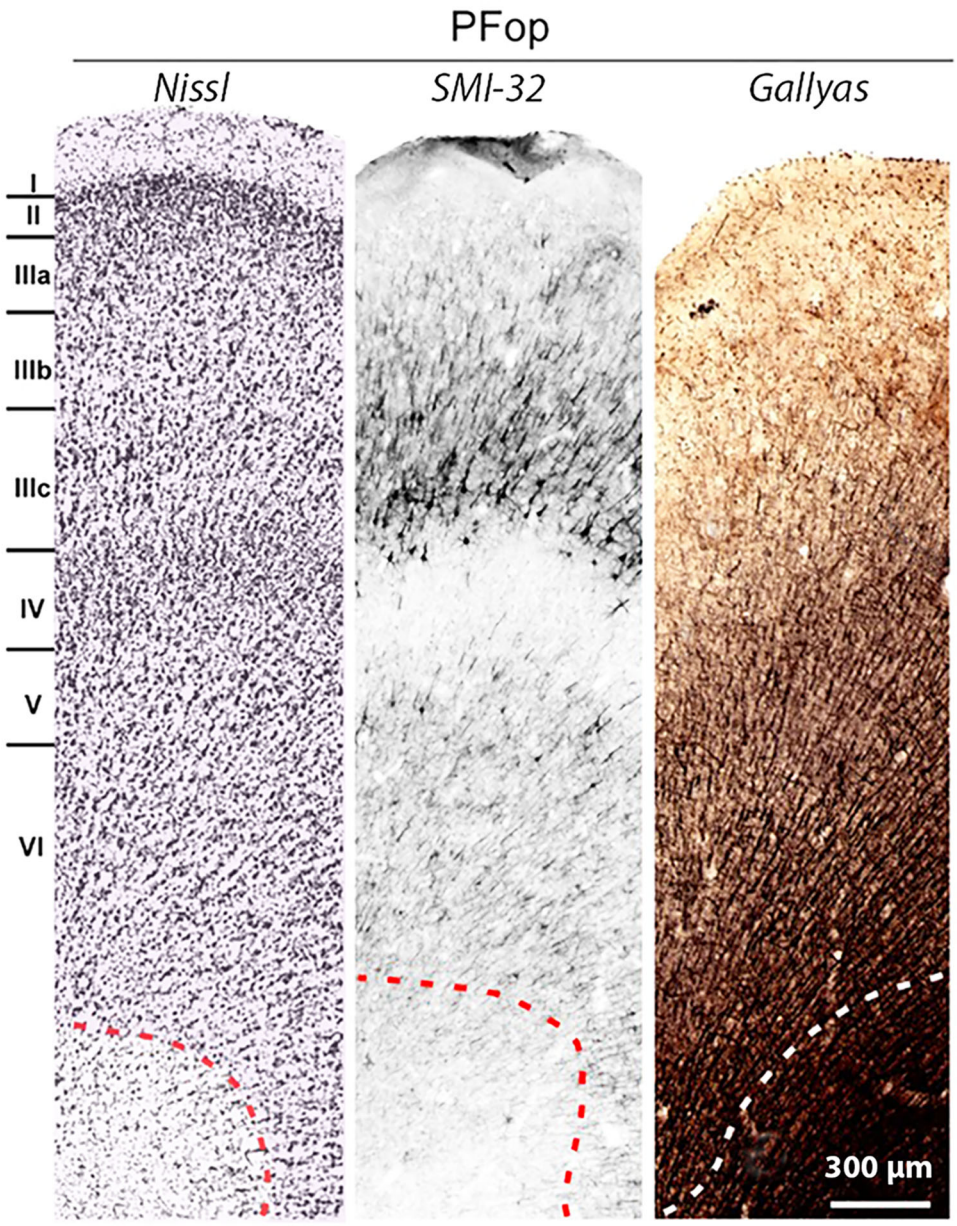

FIGURE 6 Characterization of area PFop based on cytoarchitecture, SMI-32 immunostaining and myeloarchitecture. Enlargement of the regions of area PFop encompassed by the blue dashed rectangles shown in Figures 2–4. Red or white dashed lines indicate the boundary between gray and white matters

and b). At higher magnification (Figure 7), we can observe a radial arrangement of the cells across layers IIIb and IV. Layer III can be stratified into upper (a) and lower (b) sublayers. The former showed a greater density of small cells, while the later showed sparsely distributed medium and large cells. Layer V of area PG was more discernible than the one of area PFG. Additionally, the former contained relatively more scattered medium pyramidal neurons than the later. Layer VI is populated by small cell bodies.

Layer II in area PGop showed more intense cell staining and more cell bodies than the corresponding layer II of area PG (Figures 2b and 8). PGop's layer III showed a denser distribution of pyramidal neurons in its lower sublayer, while the cell bodies of PG's layer III are more homogeneously distributed. On the other hand, layers IV, V, and VI of areas PGop and PG are quite similar. Regarding layer V, both areas show medium pyramidal cells sparsely distributed, while layer VI is populated by small cell bodies.

SMI-32 immunostaining allows us to compare layer III of areas PG and PFG (Figure 3b and 7). Layer III of area PG is more compact and shows greater labeling intensity than layer III of area PFG. Greater magnification allowed us to observe that layer III was thinner in PG as compared to PFG. Despite this fact, it could still be stratified into sublayers a and b, where sublayer b showed a greater density of large and sparse cells than sublayer a. Layers V and VI in both areas also showed somewhat clear boundaries between them. Layer V contains

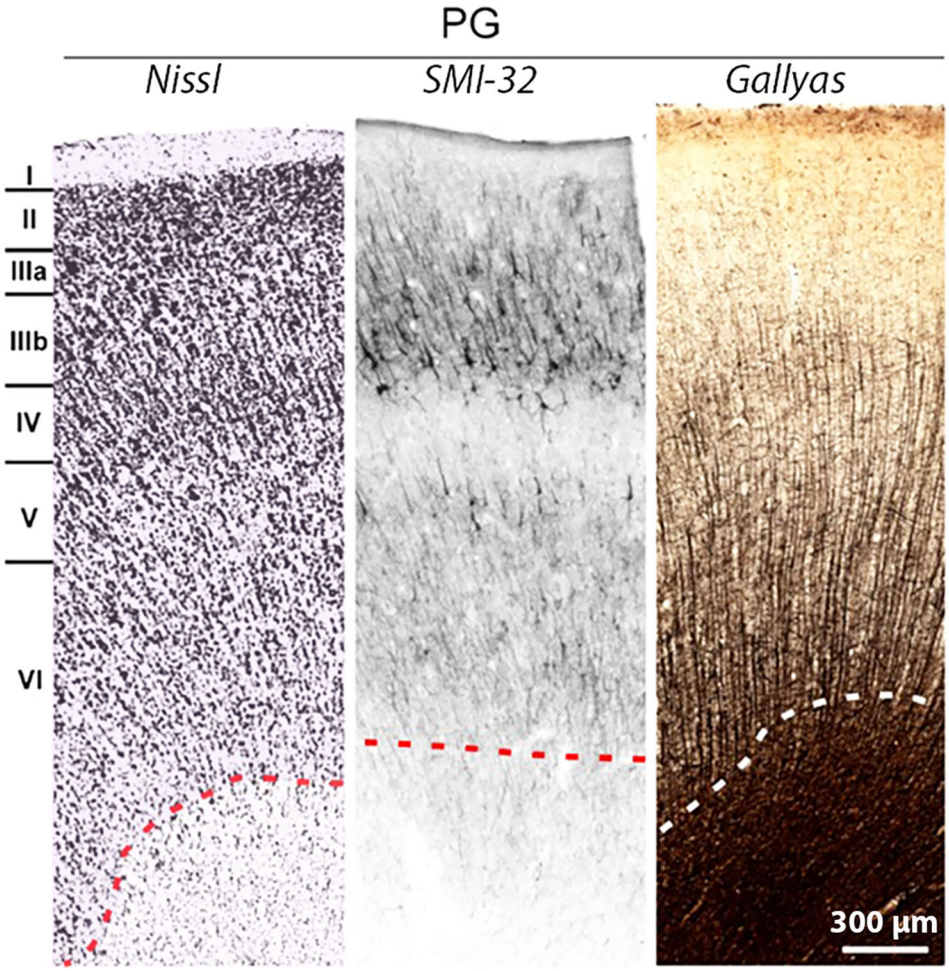

FIGURE 7 Characterization of area PG based on cytoarchitecture, SMI-32 immunostaining and myeloarchitecture. Enlargement of the regions of area PG encompassed by the blue dashed rectangles shown in Figures 2–4. Red or white dashed lines indicate the boundary between gray and white matters

medium-sized pyramidal neurons, but with more apparent apical dendrites, while layer VI contained few small labeled neurons and some labeled neuropil.

Area PGop shows fewer labeled neurons in layer III and in the infragranular layers relative to area PG. The infragranular layers exhibits a lower cell density and sparser apical dendrites. Layer III in PGop could also be stratified into sublayers a, showing characteristic apical dendrites, and sublayer b, containing small pyramidal cells. Layer V shows few stained cells and almost no apical dendrites, while layer VI showed weak neuropil immunostaining, as is observed in area PFG (Figures 3b and 8).

Myelin staining revealed that area PG has the same vertical arrangement of fiber bundles as observed in PGop, but with a more prominently thick and sparse pattern (Figures 4b and 7). In addition, the outer and inner bands of Baillarger are more prominent in PG than PGop (compare Figures 7 and 8). Overall, PG and PGop can be architecturally distinguished from areas PFG and PFop due to their vertically oriented fiber bundles, resembling a radial pattern.

Area Opt

Area Opt is the most medial area we describe in IPC. In Nissl-stained sections, layer II presented a high density of cell bodies (Figure 2c). At higher magnification (Figure 9), we observe a radial pattern of vertically clustered cells, which was found to be even more pronounced than the one we find in area PG. The medium-sized pyramidal cells in layer III are sparsely arranged along the entire layer. Layer IV presents a high density of small granule cells and a clear boundary with layer V. However, we do not find a clear boundary between layers V and VI.

Layer III of area Opt shows few cells immunostained for SMI-32, at least when compared to area PG (Figure 3c). At higher magnification (Figure 9), we observe that layers III and V contain sparsely distributed pyramidal cells with long apical dendrites, highlighting its radial pattern. In general, the layer III is more densely populated by large pyramidal neurons than layer V that showed sparse pyramidal cells and few apical dendrites invading layer IV.

Myelin staining shows that area Opt contains prominent fiber bundles that are more vertically oriented than those found in the more lateral IPC areas. Additionally, the outer and inner bands of Baillarger in

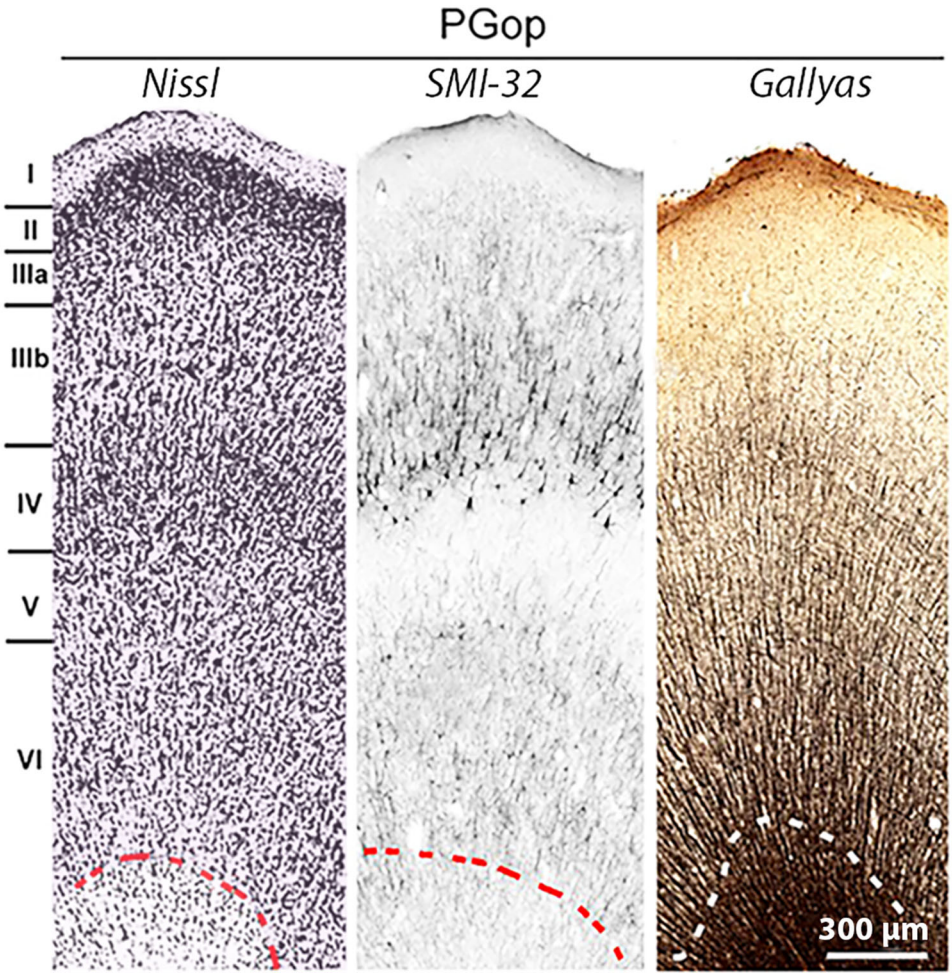

FIGURE 8 Characterization of area PGop based on cytoarchitecture, SMI-32 immunostaining and myeloarchitecture. Enlargement of the regions of area PGop encompassed by the blue dashed rectangles shown in Figures 2–4. Red or white dashed lines indicate the boundary between gray and white matters

area Opt are less evident than those in the lateral IPC areas (Figures 4c and 9).

4 | DISCUSSION

Skilled hands movements, including the goal-directed use of tools is a distinctive behavior observed in primates. Capuchin monkeys stand out among New-World monkeys (and Old-World monkeys alike) in their elaborate ability for the manual use of tools. The inferior parietal cortex (IPC) is involved in the sensorimotor integration processes that underline hand movements, including tool manipulation. It is therefore paramount that we understand the cortical organization of the IPC, including the number of cortical areas it contains, and whether the capuchin monkey exhibits any architectural features that differentiate it from other primates. To this aim, immunostaining techniques with the potential to reveal unique architectural features across cortical areas are invaluable tools in our effort to adequately parcellate the IPC. In this way, SMI-32 immunostaining (Sternberger & Sternberger, 1983) has been used for cortical parcellation in different mammalian groups, such as rodents (Boire et al., 2005; Dias et al., 2014; Van der Gucht et al., 2007), Old-World monkeys (Ding et al., 2009; Gregoriou et al., 2006; Lewis & Van Essen, 2000) and New-World monkeys (Cruz-Rizzolo et al., 2011, Mayer et al., 2016, 2019; Mariani et al., 2019). Similar to what has been observed in macaques (Campbell & Morrison, 1989; Hof & Morrison, 1995; Hof et al., 1996; Lewis & Van Essen, 2000; Lewis et al., 1999), SMI-32 immunohistochemistry in the capuchin monkey reveals a heterogeneous cortical labeling pattern, where two bands with varying levels of immunoreactivity are usually observed in layers III and V (Cruz-Rizzolo et al., 2011; Soares et al., 2008). These two bands are composed of small to large pyramidal neurons, including their proximal processes and apical dendrites.

The laminar distribution of cell bodies and dendrites are the main criteria used to differentiate among the cortical areas of the capuchin monkey. Regarding SMI-32 and Nissl staining, anatomical features such as the size, density, laminar distribution and labeling intensity of cell bodies are important. SMI-32 immunostaining allows us to evaluate additional anatomical criteria, such as the thickness of apical dendrites, the relative neuropil staining across cortical layers, the relative thickness of cortical layers, and the breakup of cortical layers into sublayers.

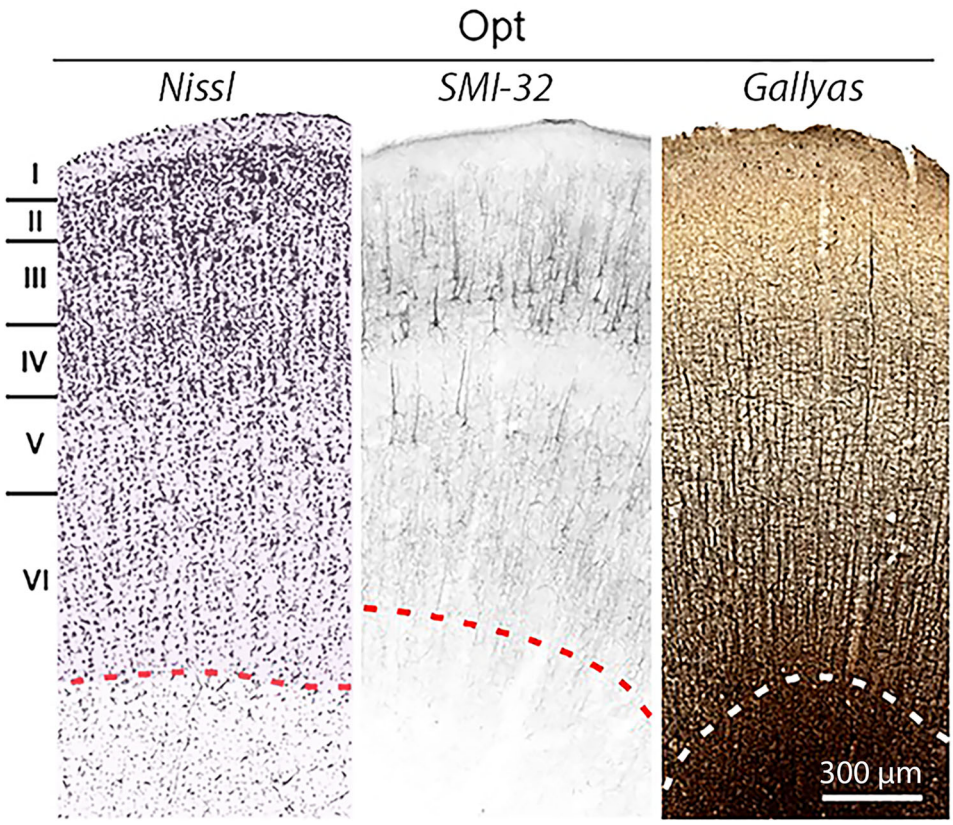

FIGURE 9 Characterization of area Opt based on cytoarchitecture, SMI-32 immunostaining and myeloarchitecture. Enlargement of the regions of area Opt encompassed by the blue dashed rectangles shown in Figures 2–4. Red or white dashed lines indicate the boundary between gray and white matters

These criteria have been successfully used to describe cortical organization in humans (Caspers et al., 2006; Eickhoff et al., 2006), Old-World monkeys (Gregoriou et al., 2006; Morecraft et al., 2012; Pandya & Seltzer, 1982), and New-World capuchin monkeys (Cruz-Rizzolo et al., 2011; Mayer et al., 2016, 2019; Mariani et al., 2019). Notably, studies have shown that cortical parcellation based on cytoarchitecture correlates well with neurotransmitter receptor distribution in monkeys (Geyer et al., 2005; Niu et al., 2020, 2021) and humans (Caspers et al., 2013).

There is a notable difference in the inclination of the intraparietal sulcus between capuchin and macaque monkeys. If we estimate the relative angle between this sulcus and the coronal plane, the intraparietal sulcus in capuchins is more parallel oriented relative to the coronal plane, as compared to macaque monkeys, where the intraparietal sulcus is more obliquely disposed. Based on these characteristics, the lateral region of capuchin IPC is analogous to the rostral region of macaque IPC. In the macaque, the most rostral area of IPC is area PF. Accordingly, in both macaque and capuchin monkeys, the opercular areas PFop and PGop share borders with areas PFG and PG, respectively. However, areas PFop e PGop in the capuchin share rostral borders with PFG and PG, respectively, while in the macaque these borders are localized medially. Area PG is located medially relative to area PFG, and we found area Opt to be the most medially located area in capuchin IPC. On the other hand, the anatomical disposition of the intraparietal sulcus in the capuchin and the fact that we sliced the cortex parasagittally impaired us from appropriately examining area PF due to its far lateral position in the brain (region lateral to area PFG in Figure 1). Future work should try to revisit this issue using another sectioning plane. Taken together, we suggest that the intraparietal sulcus should be used as an anatomic reference when pairing corresponding IPC areas between macaque and capuchin monkeys (Andersen et al., 1997; Matelli et al., 1998; Morecraft et al., 2012; Pandya & Seltzer, 1982; Petrides & Pandya, 2007; Rozzi et al., 2006; Seltzer & Pandya, 1984; Seltzer & Pandya, 1986; Zhong & Rockland, 2003) and electrophysiological studies (Hyvärinen, 1981; Hyvärinen & Shelepin, 1979; Leinonen et al., 1979a, 1979b; Yokochi et al., 2003; Battaglia-Mayer et al., 2015; Rozzi et al., 2008).

4.1 | Comparison of New- and Old-World monkeys

The two initial works that employed SMI-32 immunolabeling to study macaque IPC parceled it into two distinct cortical regions: area 7a and area 7b (Lewis & Van Essen, 2000 and Hof & Morrison, 1995). Subsequently, Gregoriou et al. (2006), also using SMI-32 immunolabeling, were able to parcel macaque IPC into four areas, namely areas PF, PFG, PG and Opt. However, work Pandya and Seltzer (1982) using cytoarchitectonic, myeloarchitectonic and connectivity, was able to parcel

macaque IPC into the 6 areas: the four areas described by Gregoriou et al. (2006) and two additional areas that they named PFop and PGop. The work of Niu et al. (2021), using neurotransmitter receptor distribution, confirmed the results of Pandya and Seltzer (1982). Our results in the capuchin monkey using cytoarchitectonic, myeloarchitectonic, and SMI-32 immunohistochemistry corroborate the results of Pandya and Seltzer (1982) and Niu et al. (2021), even though we were not able to study area PF due to the technical reasons mentioned above. Below, we discuss the characteristics of the each of the five IPC areas that we describe in this work.

4.1.1 | Area PFG

We observed that cortical layers II, V, and VI in area PFG of the capuchin have higher cell densities than its counterparts in the macaque (Geyer et al., 2005; Gregoriou et al., 2006; Pandya & Seltzer, 1982; Rozzi et al., 2006). Furthermore, PFG in the capuchin does not present a cortical lamination pattern that resembles a radial arrangement like we observed in the more medial IPC areas of the capuchin or as observed by other authors in area PG of the macaque (Geyer et al., 2005; Gregoriou et al., 2006; Pandya & Seltzer, 1982; Rozzi et al., 2006). Pandya and Seltzer (1982) described area PFG as having a higher density of cell bodies and a clearer laminar profile compared to area PF, in addition to exhibiting a radial pattern. Pandya and Seltzer (1982) considered PFG as a transition area between PF and PG. On the other hand, Gregoriou et al. (2006) disagreed with this interpretation and considered PFG as a unique and well-delimited cortical area. It is important to note that Pandya and Seltzer (1982) used only coronal sections for their analysis, while Gregoriou et al. (2006) used coronal, perpendicular and parallel to the intraparietal sulcus in order to study the IPC.

4.1.2 | Area PFop

Pandya and Seltzer (1982) observed that the macaque area PFop does not have a radial appearance as found in area PF. Additionally, PFop has comparatively fewer larger cells in sublayer IIIc. In terms of myeloarquitecture, layer IV PFop is poorly differentiated from layer III. Finally, these authors reported that area PFop has an outer band of Baillarger and an inner plexus of fibers. There are few studies that make use of immunostaining techniques to study the opercular areas of the IPC. Based on immunohistochemistry for SMI-32, Lewis and Van Essen (2000) described a single area in the macaque IPC operculum (area 7op), which is adjacent to area 7a and characterized as having a higher cell density compared to area 7a. In the capuchin, we observe that layer III of area PFop shows a higher density for medium and large cells compared to PGop, while PFop layer V is similar to the one in area PFG, with small and medium pyramidal cells arranged sparsely. Areas PFop and PGop in the macaque are connected to area F3 in the frontal lobe (Luppino et al., 1993) and to area PE in the parietal lobe (Bakola et al., 2013).

4.1.3 | Area PG

Area PG in the capuchin monkey exhibits clusters of cell bodies in a radial arrangement, similar to what has been described in macaque area PG by other authors (Geyer et al., 2005; Gregoriou et al., 2006; Rozzi et al., 2006). Curiously, Pandya and Seltzer (1982) described area PG as having the least radial appearance among the IPC areas, with a more homogeneous appearance compared to areas PF and PFG. This was mainly because area PG shows comparatively weak staining of large cell bodies in layers III and V. In the capuchin monkey we observe intensely stained cell bodies in area PG, allowing us to draw clear boundaries between the cortical layers, including layer III, which is sparsely populated by medium and large cells. Geyer et al. (2005) report that layer III of area PG has a discrete gradient of cell body staining along its sublayers. They observed that layer IIIc is not as populated by large cells as the rostral areas of the IPC, but it has a high density of small cell bodies in all layers. In capuchins were observe that area PG has the thinnest layer III of all IPC areas, and that its layer III cells are less sparse compared to layer III of area PFG. Sublayer IIIb contains mostly medium and large neurons, with apical dendrites that project to the most superficial portion of this layer. Layer V of both PFG and PG have similar densities of small and medium cells, with their apical dendrites sparsely arranged (Figures 5 and 7). According to Gregoriou et al. (2006), layer III of macaque area PG exhibits weaker SMI-32 immunostaining for pyramidal cells and apical dendrites as compared to area PFG. Furthermore, they report that the apical dendrites of pyramidal neurons in sublayer IIIc of area PG are smaller compared to the same sublayer in area PFG. Finally, Gregoriou et al. (2006) report that layer V immunostaining is weaker in PG compared to PFG, and is characterized by small pyramidal neurons and weakly labeled neuropil.

4.1.4 | Area PGop

We observe that area PGop in the capuchin exhibits well defined cortical layers. This is especially true for layers II and IV, which show a higher cell body density compared to layers II and IV of area PFop. This is similar to what has been observed in macaque PGop, which also exhibits well defined cortical layers (especially layers II and IV with its higher cell densities) compared to area PFop (Pandya & Seltzer, 1982; Pandya et al., 2015). Pandya et al. (2015) described large and sparse pyramidal cells in layer IIIc of area PGop, similar to what we found in the inner most sublayer of layer III of the capuchin monkey.

4.1.5 | Area Opt

The cells of area Opt in the capuchin monkey are disposed in a radial arrangement that is even more pronounced than the one found in area PG. Layer III of area Opt in the macaque was also described as having a radial arrangement has (Gregoriou et al., 2006; Rozzi et al., 2006). Andersen et al. (1990a) highlighted the radial cell arrangement of the macaque area 7a (probably corresponding to area Opt) using Nissl

staining. In our study, layer III of area Opt is thinner than layers III of areas PFG and PG. However, no obvious subdivisions of layer III are observed because its large cell bodies are sparsely distributed throughout the layer. According to Pandya and Seltzer (1982), supragranular and infragranular layers of area Opt in the macaque have approximately the same cell density. However, there was no clear evidence for large pyramidal neurons in layer IIIc, as had been observed in area PG. Layer V was reported to have small to medium sized cells, even though other studies have reported large cell bodies in sublayer IIIc of area Opt in the macaque (Gregoriou et al., 2006; Rozzi et al., 2006). In accordance with our study in the capuchin, Nissl staining also does not reveal well-defined limits between layers IV and V, and between V and VI in the macaque (Pandya & Seltzer, 1982).

In our work, SMI-32 immunostaining shows large (albeit sparsely distributed) pyramidal neurons in layer III of area Opt, with long apical dendrites that project to layer II. However, its cell density is lower than the one found in area PG. Layer V of area Opt is also characterized by sparsely distributed neurons and the corresponding apical dendrites, but the cell bodies are comparatively smaller than in layer III (Figure 9). Lewis and Van Essen (2000) described area 7a in the macaque as showing low immunoreactivity for the SMI-32 antibody. However, they observed a radial laminar orientation of the cells and dendrites in layers III and V. Similar to the Nissl staining described above, SMI-32 immunostaining in area Opt of the capuchin monkey also reveals that the pyramidal neurons and their corresponding apical dendrites in layers III and V have a vertical orientation, in accordance with what Hof and Morrison (1995) described for area 7a in the macaque. SMI-32 immunostaining performed by Gregoriou et al. (2006) characterized macaque area Opt as having a lower density of large pyramidal neurons in layer IIIc as compared to area PG. This description is similar to the one we offer here for capuchin area Opt.

Reyes et al. (2022) recently studied the cytoarchitecture, myeloarchitecture, and parcellation of the chimpanzee inferior parietal lobe. They identified four major areas on the lateral convexity of the chimpanzee IPL (PF, PFG, PG, OPT), in addition to two opercular areas (PFOP, PGOP), similar to what has been described for the macaque. The authors thereby suggest that chimpanzees share homologous IPL areas with the macaque. In comparison, they argue that rostral IPL in humans differ in its anatomical organization and contain additional subdivisions, such as areas PFt and PFm described by Caspers et al. (2006).

5 | CONCLUSION

Our subdivision of the inferior parietal cortex (IPC) in the New-World capuchin monkey is in accordance with the one proposed for the Old-World macaque monkey. We describe a total of five areas: PFG, PG, Opt, PFop, and PGop. The first three areas are located in the convexity of the IPC, while the latter two areas are located in the IPC operculum. Area PF, the most lateral-anterior area of the IPC (Gregoriu et al., 2006; Niu et al., 2021; Pandya & Seltzer, 1982) could not be investigated in the present study due to technical reasons. The IPC areas in both species share distinct levels of similarity between them. PFG is the area most different between Old- and New-World monkeys, especially regarding cell density in layers II and IV. On the other hand, area Opt was the most similar between the two monkey groups. This similarity was evident in SMI-32 immunostaining, which revealed large and sparsely distributed pyramidal neurons that vertically project their apical dendrites to the supragranular layer. Area PG was also quite similar between the Old- and New-World monkey groups, as evidenced by the clusters of radially oriented cell bodies. Unfortunately, we could not compare the two opercular areas we describe in the capuchin monkey (i.e., areas PFop and PGop) with those described in the macaque. This is because Pandya and Seltzer (1982) did not provide in their work any figure for these corresponding regions. Overall, our data indicate a strong homology of the IPC in Old- and New-World primates. The more subtle anatomical differences we observe between both groups may be related to interspecific variability or to yet unknown behavioral demands linked to differential use of skilled hand movements.

AUTHOR CONTRIBUTIONS

All authors have full access to all the data in the study and take responsibility for the integrity of the data and the accuracy of the data analysis. Study concept and design: VB, AM, JGF. Acquisition of data: VB, JGF, AM, MLNS, JGMS. Analysis and interpretation of data: VB, RG. VB and RG prepared the illustrations. Drafting of the article: RG. Critical revision of the article for important intellectual content: RG, VB, BL, JGMS, MLNS, AM. Funding obtained by RG and JGF. Study supervision: JGF and BL.

ACKNOWLEDGMENTS

This study is part of the Master Dissertation of Vânio Bonfim da Silva (VB), who was affiliated with the Graduate Program in Biological Sciences—Physiology at the Federal University of Rio de Janeiro (UFRJ, https://www.posgraduacao.biof.ufrj.br/en). This article was done under the supervision of Professor João Guedes da Franca. His contribution to this article was fundamental. Unfortunately, João G. Franca passed away before this manuscript was finished and was thereby not able to approve its final version. That is the sole reason Prof. Franca is not listed as an author.

CONFLICT OF INTEREST

All coauthors have seen and agree with the contents of the manuscript. They declare no conflict of interest, either financial, personal, or of any other nature with persons or organizations that could inappropriately influence the results or the interpretation of the data in the article. We certify that the submission is original work and is not under review at any other journal.

DATA AVAILABILITY STATEMENT

Data have not been shared. Our web repository is under construction. Data is available upon request to the corresponding author. Text and figures are available as supplementary data.

IN MEMORIAM OF PROFESSOR DEEPAK N. PANDYA

Professor Deepak N. Pandya made important contributions to the anatomy and connectivity of the parietal cortex in macaque monkeys. He also made outstanding contributions on the cortical connections in primates, and on comparative brain architectonics in the monkey and human. His great scientific expertise and rigorous application of anatomical techniques will be always remembered.

ORCID

Ricardo Gattass https://orcid.org/0000-0002-0321-1490

PEER REVIEW

The peer review history for this article is available at https://publons.com/publon/10.1002/cne.25449.

REFERENCES

Andersen, R. A., Asanuma, C., Essick, G., & Siegel, R. M. (1990a). Corticocortical connections of anatomically and physiologically defined subdivisions within the inferior parietal lobule. *Journal Comparative Neurology*, *296*, 65–113. https://doi.org/10.1002/cne.902960106. PMID: 2358530.

Andersen, R. A., Bracewell, R. M., Barash, S., Gnadt, J. W., & Fogassi, L. (1990b). Eye position effects on visual, memory, and saccade-related activity in areas LIP and 7a of macaque. *Journal of Neuroscience*, *10*, 1176–1196. https://doi.org/10.1523/JNEUROSCI.10-04-01176.1990

Andersen, R. A. (1997). Multimodal integration for the representation of space in the posterior parietal cortex. *Philosophical Transactions of the Royal Society (London)*, *352*, 1421–1428. https://doi.org/10.1098/rstb.1997.0128

Asanuma, C., Andersen, R. A., & Cowan, W. M. (1985). The thalamic relations of the caudal inferior parietal lobule and the lateral prefrontal cortex in monkeys: Divergent cortical projections from cell clusters in the medial pulvinar nucleus. *The Journal of Comparative Neurology*, *241*, 357–381. https://doi.org/10.1002/cne.902410309

Bakola, S., Passarelli, L., Gamberini, M., Fattori, P., & Galletti, C. (2013). Cortical connectivity suggests a role in limb coordination for macaque area PE of the superior parietal cortex. *The Journal of Neuroscience*, *33*, 6648–6658. https://doi.org/10.1523/JNEUROSCI.4685-12.2013

Battaglia-Mayer, A., Mascaro, M., Brunamonti, E., & Caminiti, R. (2015). The over representation of contralateral space in parietal cortex: A positive image of directional motor components of neglect? *Cerebral Cortex*, *15*, 514–525. https://doi.org/10.1093/cercor/bhh151

Bezgin, G., Wanke, E., Krumnack, A., & Kötter, R. (2008). Deducing logical relationships between spatially registered cortical parcellations under conditions of uncertainty. *Neural Network*, *21*, 1132–1145. https://doi.org/10.1016/j.neunet.2008.05.010

Bezgin, G., Vakorin, V. A., van Opstal, A. J., Mcinstosh, A. R., & Bakker, R. (2012). Hundreds of brain maps in one atlas: Registering coordinate-independent primate neuro-anatomical data to a standard brain. *NeuroImage*, *62*, 67–76. https://doi.org/10.1016/j.neuroimage.2012.04.013

Boire, D., Desgent, S., Matteau, I., & Ptito, M. (2005). Regional analysis of neurofilament protein immunoreactivity in the hamster's cortex. *Journal of Chemical Neuroanatomy*, *29*, 193–208. https://doi.org/10.1016/j.jchemneu.2005.01.003

Brodmann, K. (1905). Beiträgezur histologischen Lokalisation der Grosshirnrinde. Dritte Mitteilung: Die Rindenfelder der niederen Affen. *Journal Psychology Neurology Lpz*, *4*, 177–226.

Buneo, C. A., & Andersen, R. A. (2006). The posterior parietal cortex: Sensorimotor interface for the planning and online control of visually guided movements, *Neuropsychologia*, *44*, 2594–2606. https://doi.org/10.1016/j.neuropsychologia.2005.10.011

Campbell, M. J., & Morrison, J. H. (1989). Monoclonal antibody to neurofilament protein (SMI-32) labels a subpopulation of pyramidal neurons in the human and monkey neocortex. *The Journal of Comparative Neurology*, *282*, 191–205. https://doi.org/10.1002/cne.902820204

Caspers, S., Geyer, S., Schleicher, A., Mohlber, H., Amunts, K., & Zilles, K. (2006). The human inferior parietal cortex: Cytoarchitectonic parcellation and interindividual variability. *NeuroImage*, *33*, 430–448. https://doi.org/10.1016/j.neuroimage.2006.06.054

Caspers, S., Schleicher, A., Bacha-Trams, M., Palomero-Gallagher, N., Katrin, A., & Zilles, K. (2013). Organization of the human inferior parietal lobule based on receptor architectonics. *Cerebral Cortex*, *23*, 615–628. https://doi.org/10.1093/cercor/bhs048

Chaplin, T. A., Hsin-Hao, Y., Soares, J. G. M., Gattass, R., & Rosa, M. G. P. (2013). A Conserved pattern of differential expansion of cortical areas in simian primates. *The Journal of Neuroscience*, *33*, 15120–15125. https://doi.org/10.1523/JNEUROSCI.2909-13.2013

Clower, D. M., West, R. A., Lynch, J. C., & Strick, P. L. (2001). The inferior parietal lobule is the target of output from the superior colliculus, hippocampus, and cerebellum. *The Journal of Neuroscience*, *21*, 6283–6329. https://doi.org/10.1523/JNEUROSCI.21-16-06283.2001

Cruz-Rizzolo, R. J., de Lima, M. A. X., Ervolino, E., de Oliveira, J. A., & Casatti, C. A. (2011). Cyto-, myelo- and chemoarchitecture of the prefrontal cortex of the Cebus monkey. *BMC Neuroscience*, *12*, 6. https://doi.org/10.1186/1471-2202-12-6

Dias, I. A., Bahia, C. P., Franca, J. G., Houzel, J. C., Lent, R., Mayer, A. O., Santiago, L. F., Silveira, L. C. L., Picanço-Diniz, C. W., & Pereira, A. (2014). Topography and architecture of visual and somatosensory areas of the agouti. *Journal of Comparative Neurology*, *522*, 2576–2593. https://doi.org/10.1002/cne.23550

Ding, S.-L., Van Hoesen, G. W., Cassell, M. D., & Poremba, A. (2009). Parcellation of human temporal polar cortex: A combined analysis of multiple cytoarchitectonic, chemoarchitectonic, and pathological markers. *Journal Comparative Neurology*, *514*, 595–623. https://doi.org/10.1002/cne.22053

Eickhoff, S. B., Schleicher, A., Zilles, K., & Amunts, K. (2006). The human parietal operculum. I. Cytoarchitectonic mapping of subdivisions. *Cerebral Cortex*, *16*, 254–267. https://doi.org/10.1093/cercor/bhi105

Fogassi, L., & Luppino, G. (2005). Motor functions of the parietal lobe. *Current Opinions in Neurobiology*, *15*, 626–631. https://doi.org/10.1016/j.conb.2005.10.015

Friedman, H. R., & Goldman-Rakic, P. S. (1994). Coactivation of prefrontal cortex and inferior parietal cortex in working memory tasks revealed by 2DG functional mapping in the rhesus monkey. *Journal of Neuroscience*, *14*, 2775–2788. https://doi.org/10.1523/JNEUROSCI.14-05-02775.1994

Galletti, C., Gamberini, M., Kutz, D. F., Baldinotti, I., & Fattori, P. (2005). The relationship between V6 and PO in macaque extrastriate cortex. *European Journal of Neuroscience*, *21*, 959–970. https://doi.org/10.1111/j.1460-9568.2005.03911.x

Gallyas, F. (1979). Silver staining of myelin by means of physical development. *Neurology*, *1*, 203–209.

Geyer, S., Luppino, G., Ekamp, H., & Zilles, K. (2005). The macaque inferior parietal lobule: cytoarchitecture and distribution pattern of serotonin 5-HT1A binding sites. *Anatomy and Embryology (Berlin)*, *210*, 353–362. https://doi.org/10.1007/s00429-005-0026-4

Gregoriou, G. G., Borra, E., Matelli, M., & Luppino, J. (2006). Architectonic organization of the inferior parietal convexity of the macaque monkey. *The Journal of Comparative Neurology*, *496*, 422–451. https://doi.org/10.1002/cne.20933

Hof, P. R., & Morrison, J. H. (1995). Neurofilament protein defines regional patterns of cortical organization in the macaque monkey visual system—A quantitative immunohistochemical analysis. *The Journal of Comparative Neurology*, *352*, 161–186. https://doi.org/10.1002/cne.903520202

Hof, P. R., Ungerleider, L. G., Webster, M. J., Gattass, R., Adams, M. M., Sailstad, C. A., & Morrison, J. H. (1996). Neurofilament protein is

differentially distributed in subpopulations of corticocortical projection neurons in the macaque monkey visual pathways. *The Journal of Comparative Neurology*, *376*, 112–127.

Hyvärinen, J. (1981). Regional distribution of functions in parietal association area 7 of the monkey. *Brain Research*, *206*(n. 2), 287–303. https://doi.org/10.1016/0006-8993(81)90533-3

Hyvärinen, J., & Shelepin, Y. (1979). Distribution of visual and somatic functions in the parietal associative area 7 of the monkey. *Brain Research*, *169*, 561–564. https://doi.org/10.1016/0006-8993(79)90404-9

Jones, E. G., & Burton, H. (1976). Areal differences in the laminar distribution of thalamic afferents in cortical fields of the insular, parietal and temporal regions of primates. *Journal of Comparative Neurology*, *168*, 197–247. https://doi.org/10.1002/cne.901680203

Kalaska, J. F., & Rizzolatti, R. (2013). *Principles of neural science* (5th ed., p. 835). New York: McGraw Hill Medical.

Kalwani, R. M., Bloy, L., Elliott, M. A., & Gold, J I. (2009). A method for localizing microelectrode trajectories in the macaque brain using MRI. *Journal of Neuroscience Methods*, *176*, 104–111. https://doi.org/10.1016/j.jneumeth.2008.08.034

Leinonen, L., Hyvärinen, J., Nyman, G., & Linnankoski, I. (1979a). I. Functional properties of neurons in lateral part of associative area 7 in awake monkeys. *Experimental Brain Research*, *34*, 299–320. https://doi.org/10.1007/BF00235675

Leinonen, L., & Nyman, G. (1979b). II. Functional properties of cells in anterolateral part of area-7 associative face area of awake monkeys. *Experimental Brain Research*, *34*, 321–33. https://doi.org/10.1007/BF00235676

Lewis, J. W., & Van Essen, D. C. (2000). Mapping of architectonic subdivisions in the macaque monkey, with emphasis on parieto-occipital cortex. *Journal Comparative Neurology*, *428*, 79–111. https://doi.org/10.1002/1096-9861(20001204)

Lewis, J. W., Burton, H., & Van Essen, D. C. (1999). Anatomical evidence for the posterior boundary of area 2 in the macaque monkey. *Somatosensory & Motor Research*, *16*, 382–390. https://doi.org/10.1080/08990229970438

Luppino, G., Matelli, M., Camarda, R., & Rizzolatti, G. (1993). Corticocortical connections of area F3 (SMA-proper) and area F6 (pre-SMA) in the Macaque monkey. *Journal of Comparative Neurology*, *338*, 114–140. https://doi.org/10.1002/cne.903380109

Mariani, O. S. C., Lima, B., Soares, J. G. M., Mayer, A., Franca, J. G., & Gattass, R. (2019). Partitioning of the primate intraparietal cortex based on connectivity pattern and immunohistochemistry for Cat-301 and SMI-32. *The Journal of Comparative Neurology*, *527*(3), 694–717. https://doi.org/10.1002/cne.24438

Matelli, M., Govoni, P., Galletti, C., Kutz, D. F., & Luppino, G. (1998). Superior area 6 afferents from the superior parietal lobule in the macaque monkey. *Journal of Comparative Neurology*, *402*, 327–352. https://doi.org/10.1002/(SICI)1096-9861

May, J. G., & Andersen, R. A. (1986). Different patterns of corticopontine projections from separate cortical fields within the inferior parietal lobule and dorsal prelunte gyrus of the macaque. *Experimental Brain Research*, *63*, 265–278. https://doi.org/10.1007/BF00236844

Mayer, A., Nascimento-Silva, M. L., Keher, N. B., Bittencourt-Navarrete, R. E., Gattass, R., & Franca, J. G. (2016). Architectonic mapping of somatosensory areas involved in skilled forelimb movements and tool use. *Journal of Comparative Neurology*, *524*, 1399–1423. https://doi.org/10.1002/cne.23916

Mayer, A., Baldwin, M. K. L., Cooke, D. F., Lima, B. R., Padberg, J., Lewenfus, G., Franca, J. G., & Krubitzer, L. (2019). The multiple representations of complex digit movements in primary motor cortex form the building blocks for complex grip types in capuchin monkeys. *Journal of Neuroscience*, *39*(34), 6684–6695. https://doi.org/10.1523/JNEUROSCI.0556-19.2019

Morecraft, R. J., Stilwell-Morecraft, K. S., Cipolloni, P. B., Ge, J., McNeal, D., & Pandya, D. N. (2012). Cytoarchitecture and cortical connections of the anterior cingulate and adjacent somatomotor fields in the rhesus monkey. *Brain Research Bulletin*, *87*, 457–497. https://doi.org/10.1016/j.brainresbull.2011.12.005

Niu, M., Impieri, D., Rapan, L., Funck, T., Palomero-Gallagher, N., & Zilles, K. (2020). Receptor-driven, multimodal mapping of cortical areas in the macaque monkey intraparietal sulcus. *Elife*, *9*, e55979. https://doi.org/10.7554/eLife.55979

Niu, M., Rapan, L., Funck, T., Froudist-Walsh, S., Zhao, L., Zilles, K., & Palomero-Gallagher, N. (2021). Organization of the macaque monkey inferior parietal lobule based on multimodal receptor architectonics. *Neuroimage*, *231*, 117843. https://doi.org/10.1016/j.neuroimage.2021.117843

Pandya, D. N., & Seltzer, B. (1982). Intrinsic connections and architectonics of posterior parietal cortex in the rhesus monkey. *Journal of Comparative Neurology*, *204*, 196–210. https://doi.org/10.1002/cne.902040208

Pandya, D. N., Petrides, M., Seltzer, B., & Cipolloni, P B. (2015). *Cerebral cortex: Architecture, connections and the dual origin concept*. New York: Oxford University Press. https://doi.org/10.1093/med/9780195385151.001.0001

Passarelli, L., Gamberini, M., & Fattori, P. (2021). The superior parietal lobule of primates: a sensory-motor hub for interaction with the environment. *Journal of Integrative Neuroscience*, *20*, 157–171. https://doi.org/10.31083/j.jin.2021.01.334

Petrides, M., & Pandya, D. N. (2007). Efferent association pathways from the rostral prefrontal cortex in the macaque monkey. *Journal of Neuroscience*, *27*, 11573–11586. https://doi.org/10.1523/JNEUROSCI.2419-07.2007

Preuss, T. M., & Goldman-Rakic, P. S. (1991). Myelo-and cytoarchitecture of the granular frontal cortex and surrounding regions in the strepsirhine primate Galago and the anthropoid primate Macaca. *The Journal of Comparative Neurology*, *310*, 429–474. https://doi.org/10.1002/cne.903100402

Reyes, L. D., Kim, Y. D., Issa, H., Hopkins, W. D., Scott Mackey, S., & Sherwood, C. C. (2022). Cytoarchitecture, myeloarchitecture, and parcellation of the chimpanzee inferior parietal lobe. *Brain structure & function*, https://doi.org/10.1007/s00429-022-02514-w. Advance online publication.

Rizzolatti, G., Fogassi, L., & Gallese, V. (1997). Parietal cortex: From sight to action. *Current Opinion in Neurobiology*, *7*, 562–567. https://doi.org/10.1016/s0959-4388(97)80037-2

Rizzolatti, G., Luppino, G., & Matelli, M. (1998). The organization of the cortical motor system: New concepts. *Electroencephalography and Clinical Neurophysiology*, *106*, 283–296. https://doi.org/10.1016/S0013-4694(98)00022-4

Rozzi, S., Calzavara, R., Belmalih, A., Borra, H., Gregoriou, G. G., Matelli, M., & Luppino, G. (2006). Cortical connections of the inferior parietal cortical convexity of the macaque monkey. *Cerebral Cortex*, *16*, 1389–1417. https://doi.org/10.1093/cercor/bhj076

Rozzi, S., Ferrari, P. F., Bonini, L., Rizzolatti, G., & Fogassi, L. (2008). Functional organization of inferior parietal lobule convexity in the macaque monkey: Electrophysiological characterization of motor, sensory and mirror responses and their correlation with cytoarchitectonic areas. *European Journal of Neuroscience*, *28*, 1569–1588. https://doi.org/10.1111/j.1460-9568.2008.06395.x

Rushworth, M. F. S., Nixon, D., & Passingham, R. E. (1997a). Parietal cortex and movement. I. Movement selection and reaching. *Experimental Brain Research*, *117*, 292–310. https://doi.org/10.1007/s002210050224

Rushworth, M. F. S., Nixon, D., & Passingham, R. E. (1997b). Parietal cortex and movement. II. Spatial representation. *Experimental Brain Research*, *117*, 311–323. https://doi.org/10.1007/s002210050225

Seltzer, B., & Pandya, D. N. (1984). Further observations on parieto-temporal connections in the rhesus monkey. *Experimental Brain Research*, *55*, 301–312. https://doi.org/10.1007/BF00237280

Seltzer, B., & Pandya, D. N. (1986). Posterior parietal projections to the intraparietal sulcus of the rhesus monkey. *Experimental Brain Research*, *62*, 459–469. https://doi.org/10.1007/BF00236024

Soares, J. G. M., Rosado de Castro, P. H., Fiorani, M., Nascimento-Silva, S., & Gattass, R. (2008). Distribution of neurofilament proteins in the lateral geniculate nucleus, primary visual cortex, and area MT of adult Cebus monkeys. *The Journal of Comparative Neurology*, *508*, 605–614. https://doi.org/10.1002/cne.21718

Sperka, D. J., & Ditterich, J. (2011). Splash: a software tool for stereotactic planning of recording chamber placement and electrode trajectories. *Frontiers in Neuroinformatics*, *5*, 1. https://doi.org/10.3389/fninf.2011.00001

Stanton, G. B., Friedman, H. R., Dias, E. C., & Bruce, C. J. (2005). Cortical afferents to the smooth-pursuit region of the macaque monkey's frontal eye field. *Experimental Brain Research*, *165*, 179–192. https://doi.org/10.1007/s00221-005-2292-z

Sternberger, L. A., & Sternberger, N. H. (1983). Monoclonal antibodies distinguish phosphorylated and nonphosphorylated forms of neurofilaments in situ. *Proceedings of the National Academy of Sciences of the United States of America*, *80*, 6126–6130. https://doi.org/10.1073/pnas.80.19.6126

Van der Gucht, E., Hof, P. R., Van Brussel, L., Burnat, K., & Arckens, L. (2007). Neurofilament protein and neuronal activity markers define regional architectonic parcellation in the mouse. *Visual Cortex*, *Cerebral Cortex*, *17*, 2805–2819. https://doi.org/10.1093/cercor/bhm012

Van Essen, D. C., Drury, H. A., Dickson, J., Harwell, J., Hanlon, D., & Anderson, C. H. (2001). An integrated software suite for surface-based analyses of cerebral cortex. *Journal of the American Medical Informatics Association*, *8*, 443–459. https://doi.org/10.1136/jamia.2001.0080443

Van Essen, D. C. (2005). A population—Average, Landmark-and Surface-based (PALS) atlas of human cerebral cortex. *Neuroimage*, *2*, 635–662. https://doi.org/10.1016/j.neuroimage.2005.06.058

Van Essen, D. C. (2012). Cortical cartography and Caret software. *Neuroimage*, *62*, 757–764. https://doi.org/10.1016/j.neuroimage.2011.10.077

Vogt, B. A., & Gabriel, M. (1993). *Neurobiology of cingulate cortex and limbic thalamus: a comprehensive handbook* (p. 3). Urbana, IL: Springer Science + Business Media, LLC. https://doi.org/10.1007/978-1-4899-6704-6

Vogt, C., & Vogt, A. (1919). Algemeinere Ergebnisse unserer Hirnforschung. *Journal of Neurology and Psychology*, *25*, 279–461.

von Bonin, G., & Bailey, P. (1947). *The neocortex of* Macaca mulatta. Urbana, IL: University of Illinois Press.

von Economo, C., & Koskinas, G. N. (1925). *Die Cytoarchitektonik der Hirnrinde deserwachsenen Menschen*. Berlin: Springer. https://doi.org/10.1001/archneurpsyc.1926.02200300136013

Wright, K. A., Wright, B. W., Ford, S. M., Fragaszy, D., Izar, P., Norconk, M., Masterson, T., Hobbs, D. G., Alfaro, M. E., & Alfaro, J. W. L. (2015). The effects of ecology and evolutionary history on robust capuchin morphological diversity. *Molecular Phylogenetic Evolution*, *82*, 455–466. https://doi.org/10.1016/j.ympev.2014.08.009

Yokochi, H., Tanaka, M., Kumashiro, M., & Iriki, A. (2003). Inferior parietal somatosensory neurons coding face-hand coordination in Japanese macaques. *Somatosensory & Motor Research*, *20*, 115–125. https://doi.org/10.1080/0899022031000105145

Zeki, S. (2005). Introduction: Cerebral cartography 1905–2005. *Philosophical Transactions of the Royal Society, London B Biological Science*, *360*, 651–652. https://doi.org/10.1098/rstb.2005.1632

Zhong, J., Phua, D. Y. L., & Qiu, A. (2010). Quantitative evaluation of LDDMM, FreeSurfer, and CARET for cortical surface mapping. *Neuroimage*, *52*, 131–141. https://doi.org/10.1016/j.neuroimage.2010.03.085

Zhong, Y. M., & Rockland, K. S. (2003). Inferior parietal lobule projections to anterior inferotemporal cortex (area TE) in Macaque monkey. *Cerebral Cortex*, *13*, 527–540. https://doi.org/10.1093/cercor/13.5.527

How to cite this article: Bonfim, V., Mayer, A., Nascimento-Silva, M. L., Lima, B., Soares, J. G. M., & Gattass, R. (2022). Architecture of the inferior parietal cortex in capuchin monkey. *Journal of Comparative Neurology*, 1–17. https://doi.org/10.1002/cne.25449